Biophysics and Physicobiology

Special Issue: Singularity Biology and Beyond

Review Article (Invited)

Strength in numbers: Unleashing the potential of trans-scale scope AMATERAS for massive cell quantification

Taro Ichimura[1], Taishi Kakizuka[2], Yuki Sato[3], Yoichiro Fujioka[4], Yusuke Ohba[4], Kazuki Horikawa[5], Takeharu Nagai[1,2,6]

[1] *Transdimensional Life Imaging Division, Institute for Open and Transdisciplinary Research Initiatives, Osaka University, Suita, Osaka 565-0871, Japan*

[2] *Department of Biomolecular Science and Engineering, SANKEN, Osaka University, Ibaraki, Osaka 567-0047, Japan*

[3] *Department of Anatomy and Cell Biology, Graduate School of Medical Sciences, Kyushu University, Higashi-ku, Fukuoka 812-8582, Japan*

[4] *Department of Cell Physiology, Faculty of Medicine and Graduate School of Medicine, Hokkaido University, Sapporo, Hokkaido 060-8638, Japan*

[5] *Department of Optical Imaging, Advanced Research Promotion Center, Tokushima University, Tokushima 770-8503, Japan*

[6] *Research Institute for Electronic Science, Hokkaido University, Sapporo, Hokkaido 001-0020, Japan*

Singularity biology is a scientific field that targets drastic state changes in multicellular systems, aiming to discover the key cells that induce the state change and investigate the mechanisms behind them. To achieve this goal, we developed a trans-scale optical imaging system (trans-scale scope), that is capable of capturing both macroscale changes across the entire system and the micro-scale behavior of individual cells, surpassing the cell observation capabilities of traditional microscopes. We developed two units of the trans-scale scope, named AMATERAS-1 and -2, which demonstrated the ability to observe multicellular systems consisting of over one million cells in a single field of view with sub-cellular resolution. This flagship instrument has been used to observe the dynamics of various cell species, with the advantage of being able to observe a large number of cells, allowing the detection and analysis of rare events and cells such as leader cells in multicellular pattern formation and cells that spontaneously initiate calcium waves. In this paper, we present the design concept of AMATERAS, the optical configuration, and several examples of observations, and demonstrate how the strength-in-numbers works in life sciences.

◀ *Significance* ▶

This article reviews our newly developed trans-scale scope AMATERAS to promote the studies in Singularity Biology. We have realized optical imaging in a centimeter field of view with sub-cellular spatial resolution that allows dynamic observation of more than one million cells. By utilizing image analysis techniques, AMATERAS can accomplish rare cell detection in a massive cell population, their statistical analysis, and statistical analysis of all cells.

Corresponding author: Taro Ichimura, Institute for Open and Transdisciplinary Research Initiatives, Yamadaoka 2-1, Suita, Osaka 565-0871, Japan. ORCID iD: https://orcid.org/0000-0002-3740-3634, e-mail: ichimura@otri.osaka-u.ac.jp

Introduction

Singularity Biology is a novel approach to biological research that primarily focuses on drastic changes in the states of multicellular systems. These changes are triggered by singularities (specific points) involving rare cells or events. In this context, live imaging technology is crucial because it can allow for the direct capture of the moments when specific cells within a population initiate a state transition. Such transitions, which we defined as "singularity phenomena", occur in various areas of biology, including cell differentiation and tissue development [1,2], macroscale pattern oscillations such as epilepsy and arrhythmia [3,4], disease initiation such as cancer transformation and viral infection [5,6], and brain pathologies such as Alzheimer's disease [7]. In each case, direct observation of their dynamics by live imaging provides a clear and straightforward method to understand the singularity phenomena. An essential aspect of the observation system is the ability to simultaneously observe a large number of cells. The greater the number of cells observed simultaneously, the greater the likelihood of detecting a cell with a low probability of being present in the population. The performance of an imaging system is determined by its spatial resolution, which is capable of resolving a single cell while maintaining a large field of view (FOV) or observation volume.

Over the past decade, several research groups have reported the development of fluorescence live imaging devices with a large FOV and single cell resolution [8–12]. They are commonly referred to as "mesoscopes". Most of them target neuronal activity imaging in neuroscience, by combining laser-scanning two-photon excitation fluorescence imaging with a large-aperture lens system to achieve neuronal activity imaging within a FOV of a few millimeters [9–11]. A commercially available two-photon Mesoscope system from Thorlab Inc. [13] makes this technology available to the general research community. Large-aperture lens systems for single-photon excitation fluorescence imaging in the visible wavelength range have also been realized by several groups: the Mesolens system is a pioneering development in this field, with a large FOV of 6 mm and a spatial resolution of sub-micrometers [8]. Now, our goal is to image as many cells as possible to perform singularity biology. To this end, two-photon imaging systems are limited in the number of cells they can image in a single FOV. This limitation stems from their reliance on a laser scanning system, whose pixel throughput cannot exceed the frequency of the excitation pulse train and, typically capped at a few tens of megapixels per second [10,11]. In contrast, CMOS-based wide-field imaging can exceed gigapixels per second thanks to the use of a high-speed interface. In terms of optical design, the Mesolens system achieves intracellular resolution within a 6 mm FOV by choosing a 4x magnification [8]. However, aiming to encompass a greater number of cells, we opted to prioritize a larger FOV, accepting a reduction in the spatial resolution as trade-off. Consequently, we decided to design and develop our own imaging system with a lower magnification.

In this study, we have developed a novel optical imaging technique for the simultaneous observation of massive cell populations [14,15]. We categorized this type of imaging system as "trans-scale scope" because it can provide imaging of spatial information from the micrometer to the centimeter scale, covering a wide range in the scale hierarchy (trans-scale imaging). We named our instrument AMATERAS (A Multiscale/Multimodal Analytical Tool for Every Rare Activity in Singularity) and successfully developed two different systems of AMATERAS with unique configurations. The first configuration is a prototype system, assembled from commercially available components, offering a straightforward approach. The second configuration, however, is a custom-designed unique system with significantly enhanced optical performance. This paper will describe the technological aspects of the imaging systems, explain our design considerations, and provide a comparative analysis with conventional microscopes. We will also discuss the effectiveness of the system and potential contributions to biology.

Design Concept of AMATERAS

In order to realize the purpose of this study, *i.e.*, to observe the behavior of individual cells at a single cell resolution during drastic state transitions in a multicellular system, we considered how the optical performance of the imaging system should be set. Obviously, this depends on the cell type to be observed, but for eukaryotic cells we considered a resolution of less than 3 μm as the resolution at which individual cells can be observed separately. This spatial resolution is inferior to the submicron resolution of the mesoscopes of the other groups mentioned above, but it allows for a larger FOV. At this spatial resolution, features of individual cells must be visualized in order to detect characteristic cells. While shape and dynamics obtained by bright-field imaging are important features, it is also essential to visualize the molecular features of the cell (type and amount of proteins, metabolites, messenger molecules, etc.) by using fluorescent probes. For this reason, the wavelength range of observation was fixed in the visible region, where a variety of fluorescent probes (fluorescent dyes and proteins) can be used. As for the configuration of the imaging system, a wide-field illumination type was chosen instead of a laser scanning type in order to achieve high temporal resolution imaging with a large number of pixels. As for the observation modes, we designed an apparatus capable of selecting between fluorescence imaging of specific features using fluorescent labeling and bright-field illumination imaging to observe morphology and dynamics without labeling.

The key components in wide-field visible light imaging are the lens system and the image sensor. The critical factor in

(A) conventional microscope

(B) trans-scale scope

AMATERAS-1

AMATERAS-2
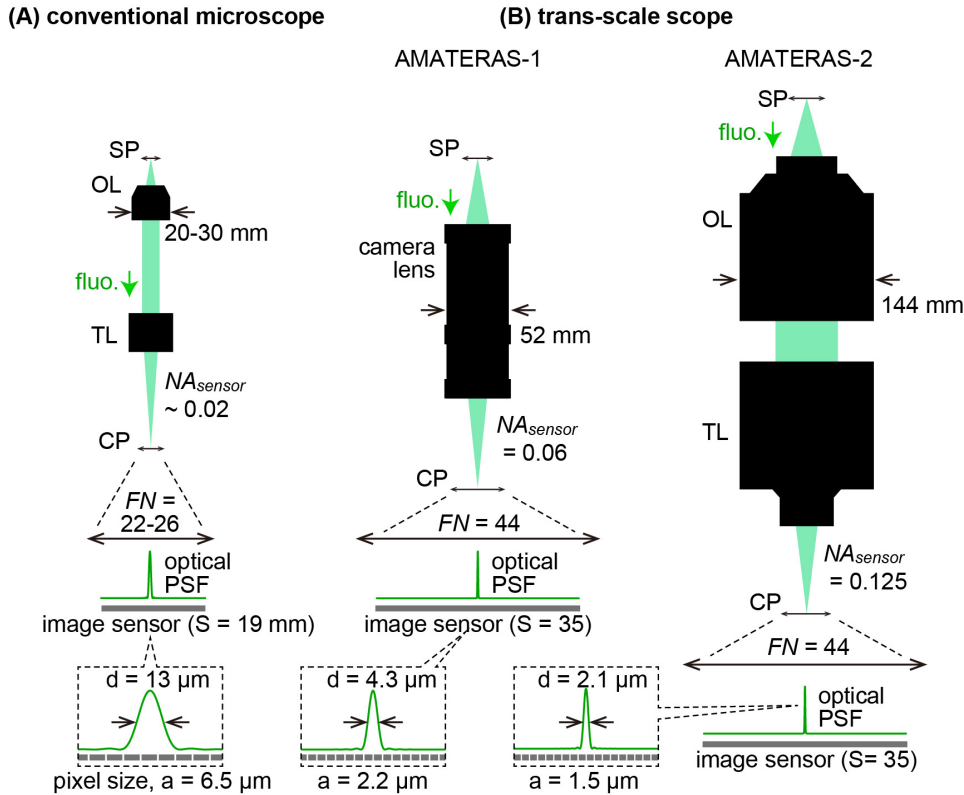
Figure 1 Schematic illustration comparing the scale dimension of the lens system and image sensor between the conventional optical microscope (A) and the two types of trans-scale scopes developed by us (B). SP: sample plane, OL: objective lens, TL: tube lens, CP: conjugate plane, *FN*: field number, NA_{sensor}: sensor-side numerical aperture, PSF: point-spread function. See main text for the details.

increasing the number of cells that can be observed in imaging is the number of sampling points that make up an image, which is equal to the number of pixels in the image sensor used. In contrast to the scientific CMOS sensors with a few megapixels typically used in conventional cell biology, some CMOS sensors used in the machine vision have a significantly higher number of pixels, such as 120 or 250 megapixels. The use of such sensors allows the generation of images with a higher number of sampling points compared to conventional microscopes.

However, because an image sensor with a large number of pixels has a large chip size, it is useless if the lens system cannot cover this size. In addition, if the spread of the point image, which depends on the performance of the lens system, is too large compared to the pixel size, adjacent pixels cannot acquire independent information. That is, the advantage of the number of pixels is reduced. Therefore, it is essential to select an optimal combination of image sensor and lens system.

In conventional biological microscopes, the numerical aperture (NA) of the lens system at the sensor side (sensor-side NA, NA_{sensor}) is at most 0.04, and typically around 0.02 (Fig. 1A). In the green wavelength region ($\lambda \sim 520$ nm), the spread of the point image on the imaging plane ($d = \lambda/2\,NA_{sensor}$) is approximately 13 µm, which is in excellent agreement with the pixel size of commonly used CMOS cameras ($a = 6.5$µm), since the pixel size is generally considered to be optimal at half the optical resolution ($a \sim d/2$). On the other hand, it is larger than the pixel sizes (2.2 µm and 1.5 µm) of 120-megapixel and 250-megapixel CMOS cameras. This means that a lens system with a larger sensor-side NA is required (Fig. 1B), which also means that the object-side NA ($NA_{obj} = M \times NA_{sensor}$; M is the magnification) must be large.

In addition, since the chip size of a CMOS sensor with a large number of pixels is also large, the lens system must have a field number (FN) that can cover the entire chip area, where FN is defined as the diameter of the FOV measured at the image plane. In fact, the size of a 120-megapixel CMOS is 29×20 mm^2 (35 mm diagonal), which is considerably larger than the FN of conventional microscope lens systems ($FN = 22 - 26$ mm), making it impossible to use the periphery of the chip area. To maximize the number of cells, the FN must be larger than the sensor size, *i.e.*, $FN \geq S$ (S: diagonal of the image sensor) (Fig. 1B).

Consequently, it is necessary to introduce or newly develop a lens with a large NA and FN. We examined the optical performance required for the lens system by considering the above mentioned two conditions, $a \sim d/2$ and $FN \geq S$, as well as the actual pixel size (2.2 µm and 1.5 µm for 120 and 250 megapixel CMOS, respectively) and chip size ($S = 35$ mm).

As a result, the required specifications for the lens system are $NA_{sensor} > 0.059$ (for 120 megapixel CMOS) and $NA_{sensor} > 0.087$ (for 250 megapixel CMOS) on the sensor side, and $FN > 35$. Since the required spatial resolution on the object side (d/M, M: magnification) is 3 μm or less, the magnification of the system is $M > 1.47$ and $M > 1.0$ for 120 megapixel and 250 megapixel CMOS sensors, respectively.

Optical Configuration of AMATERAS

As a lens system to satisfy the above conditions, we used a telecentric macro lens (LSTL20H-F, Mutron, Japan) with a magnification of 2x and $NA_{obj} = 0.12$ ($NA_{sensor} = 0.06$) in combination with a 120-megapixel CMOS camera (VCC-120CXP1M, CIS, Tokyo, Japan) to develop the first version of AMATERAS (AMATERAS-1) [14]. In addition, to achieve a higher spatial resolution and a three-dimensional resolving capability, we developed an exceptionally giant lens system (Optosigma, Tokyo, Japan) with 2x magnification and $NA_{obj} = 0.25$ ($NA_{sensor} = 0.125$) and combined it with a 250-megapixel CMOS camera (VCC-250CXP1M, CIS, Tokyo, Japan) to build the second version of AMATERAS (AMATERAS-2) [15]. Figures 2A and 2B show the schematic diagrams of the two imaging systems. These configurations provide FOVs of approximately 1.5 cm × 1 cm (14.6 mm × 10.1 mm for AMATERAS-1 and 14.7 mm × 9.4 mm for AMATERAS-2) with a spatial resolution of approximately 2.3 μm and 1.2 μm in the lateral direction, respectively. Both versions are equipped with fluorescence imaging and bright-field imaging capabilities and can be used in either or both modes as required. It is important to note here with regard to the AMATERAS-1 that fluorescence imaging is achieved by dark-field illumination. By illuminating the specimen with LED light from outside the aperture angle (7º) of the camera lens, high-contrast fluorescence imaging can be achieved with preventing excitation light from entering the camera lens. Multiple high-intensity LED light sources can be used for multi-channel fluorescence imaging without the need for a dichroic mirror [14]. On the other hand, it is difficult to achieve dark-field illumination with AMATERAS-2 because the working distance of the objective lens is not large. Therefore, two-color imaging was realized by redesigning a large-size dichroic mirror for epi-illumination. Both the AMATERAS units have motorized stages and mechanical shutters, and are controlled by a self-developed software with an autofocus function. This allows time-lapse observations of cellular dynamics under various measurement conditions (number of wavelength channels, acquisition time, imaging frequency, etc.). Further details can be found in the original papers [14,15].

Three-Dimensional Resolving Capability

In order to apply these imaging tools to a variety of specimens, it is necessary to expand not only the size of the two-dimensional FOV but also the three-dimensional (3D) volume. We have examined how to realize three-dimensional live imaging based on the optical performance of the AMATERAS-2 lens system and proposed two approaches.

The first approach is to image within a 3D volume with a wide-field imaging system and realize 3D imaging computationally; when the 3D volume is imaged, fluorescence from outside the focal plane is superimposed as background light on the fluorescence image at the focal plane. From this image, the out-of-focus fluorescence image component is estimated using a low-pass filter-based algorithm [15] and subtracted from the original image to selectively extract information at the focal plane. This method is effective when the shape of the observed object is simple and uniform, and the fluorescence image from the focal plane is not buried in the background light noise. In fact, it has been applied to the observation of quail embryogenesis to segment the ellipsoidal shape of the nuclei of vascular endothelial cells and track them in three dimensions over time [15].

On the other hand, only a limited number of cell types and organisms can satisfy the above conditions. For example, in thick samples, the fluorescence image of multiple layers overlaps in the depth direction, which can overwhelm the focal plane information. To observe such specimens, optical suppression of the background light is essential. The second approach developed for this purpose is multi-point confocal imaging (Fig. 2C), in which a disk with a pinhole array is rotated in the image plane and this plane is imaged onto the camera by a secondary relay lens system. The pinhole diameter was set to 6 μm, which is comparable to the diameter of an Airy disk at the wavelength of the green and red fluorescence in the disk plane. The performance of this method was verified by imaging chemically fixed and cleared brain slices [15]. and its application to live imaging is being considered for the future.

Number of Observable Cells

The above innovations have made it possible to resolve individual cells in a FOV that is significantly larger than that of conventional microscopes. In addition, the FOV has been extended to three dimensions. We can now discuss how many cells can be captured in a single FOV. In two-dimensional imaging, we have demonstrated the ability to image more than one million eukaryotic cells cultured on a dish substrate in a single image [14]. Figure 2D shows an observation of highly confluent MDCK cells by AMATERAS-1. In this case, the nuclei were stained with a fluorescent dye (NuceloSeeing) and the number of cells was counted by particle analysis to be approximately 1.19×10^6 in the FOV (14.6×10.1 mm^2). The average area occupied by a single cell was estimated to be approximately 11 μm square. This sample had a high confluence, but, of course, the number of cells decreases as the size of individual cells increases. Figure 2E shows an

example of the observation of iPS cell-derived cardiac cell sheets [16] by AMATERAS-2. The average cell size was approximately 61 μm square, and the cell number was 3.8×10^4, assuming that the entire FOV (14.7×9.4 mm^2) was filled with the cells (however, the actual cell sheet existed only in an area of approximately 8.4 mm diameter with a cell number of 1.5×10^4). In this case, intracellular myofibrils can be observed. In contrast, if the target organism is a bacterium such as *Escherichia coli* (*E. coli*), the number of observable cells can be much larger because each cell is smaller. Assuming that a single *E. coli* occupies an area of 1×2 μm^2, a simple estimate yields more than 70 million cells in the FOV. Note, however, that it is difficult to spatially resolve individual *E. coli* with the current AMATERAS system, so it may be necessary to spatially separate individual cells using a microwell array [17] or other means, but even so, it is still possible to observe a large number of cells simultaneously.

   In three-dimensional imaging, the potential to observe more cells is even greater because information on multiple cell layers can be obtained. For example, in mouse brain imaging, the combination with tissue clearing techniques [18] would allow for observation at depths of up to several millimeters, making it possible to observe more than 10 million neurons. However, in the case of densely distributed cells, the poor depth resolution (~12 μm) leads to inseparable overlapping of multiple cells along the depth direction. To avoid this problem, the target cells should be sparsely distributed over a distance that allows for 3D separation. A successful example is the three-dimensional time-lapse observation of vascular network formation in quail embryos realized by applying the above-mentioned computational sectioning method to AMATERAS-2 [15]. As shown in Fig. 3A, an entire embryo was observed in a single FOV, allowing the detection of more than 10,000 cells in each time frame and the tracking of cells over 24 hours of time-lapse imaging. This is a much larger number of cells compared to conventional narrow-FOV imaging where approximately 1000 vascular endothelial cells were captured in each time frame in a limited area [19]. Thanks to the ability to view the entire embryo, we can now obtain information that conventional narrow-FOV observations cannot reveal, such as the migration pathways of all cells, correlations between distant sites, and lead to the discovery of specific cells that can trigger drastic morphological changes throughout the entire embryo, which is the target of Singularity Biology.
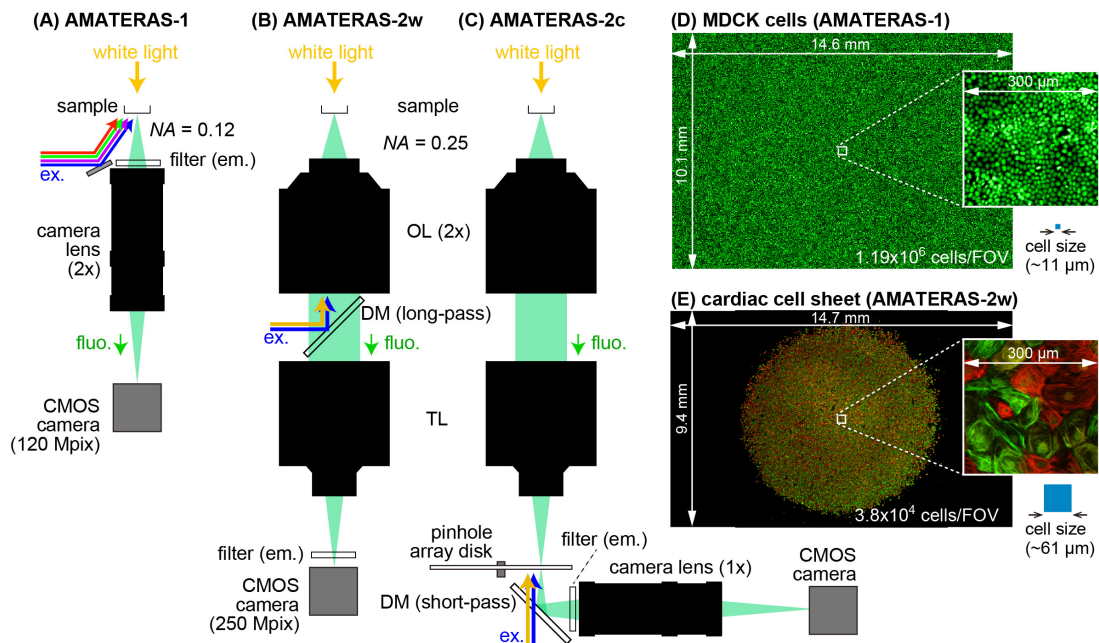

Figure 2 Optical configuration for fluorescence imaging in AMATERAS. (A) AMATERAS-1. An excitation light consisting of up to five LEDs is directed onto the sample from below with an incident angle of approximately 35 degrees. A fluorescence filter is placed at the entrance of the camera lens. (B) AMATERAS-2w, wide-field imaging configuration of AMATERAS-2. An excitation light consisting of two LEDs or lasers is introduced into the pupil plane of the objective lens through a dual-band dichroic mirror. A fluorescence filter is placed in front of the CMOS camera. (C) AMATERAS-2c, multi-point confocal imaging configuration of AMATERAS-2. A pinhole array disk is placed at the imaging plane of the tube lens. Excitation light is passed through a short-pass dichroic mirror onto the disk. The fluorescence image projected on the disk is transferred to the CMOS camera through another camera lens (1x). (D) An example of fluorescence imaging of MDCK cells stained with NucleoSeeing by AMATERAS-1. The number of cells was analyzed using a machine learning software and found to be approximately 1.19 million cells in the FOV. (E) An example of dual-color fluorescence imaging by AMATERAS-2w. A cardiac cell sheet derived from human-iPS cells was observed with immunostaining for two types of myosin light chains.

Detection of Rare Cellular Events and the Statistical Analysis

   As described above, AMATERAS increases the possibility of detecting unique cells with a low probability of existence. In fact, in a previous study elucidating spiral pattern formation in the social amoeba *Dictyostelium discoideum*, AMATERAS was able to find "leader cells" with a less than 0.2% probability of existence [14,20]. By visualizing cAMP, which induces cell chemotaxis, with a fluorescent protein indicator [21], we observed the propagation of cAMP waves over time from the early stages of the spiral formation (Fig. 3B). By retrospectively playing the time-lapse movie and searching for the origin of the spiral pattern, we revealed the mechanism of pattern formation and the cells responsible for it. This result is one of the most symbolic and remarkable achievements in this field and is expected to make a great contribution to the field.

   In addition to simply detecting rare cells, we were able to perform statistical analysis of the rare events. Simply detecting one or a few rare cells does not provide much insight into the mechanism of their occurrence. Detecting rare cells in sufficient numbers allows one to speculate about the stochastic process behind the rare cellular activity. Here we present an example of the observation of dynamically changing, spontaneous calcium transients and propagation in MDCK cells [22]. Figure 3C shows the frequency of calcium wave propagations by performing calcium imaging on MDCK cells stably expressing the fluorescent calcium indicator protein [23]. The sample had a high cell density, with approximately 1 million cells in the FOV, and only 2057 cells in 10 minutes were found to cause calcium propagation to surrounding cells. Several parameters related to the wave propagation can be quantified, including the distribution of the wave propagation area. A histogram of the propagation area shows that most calcium waves propagate only over a small area (< 5000 μm^2), while
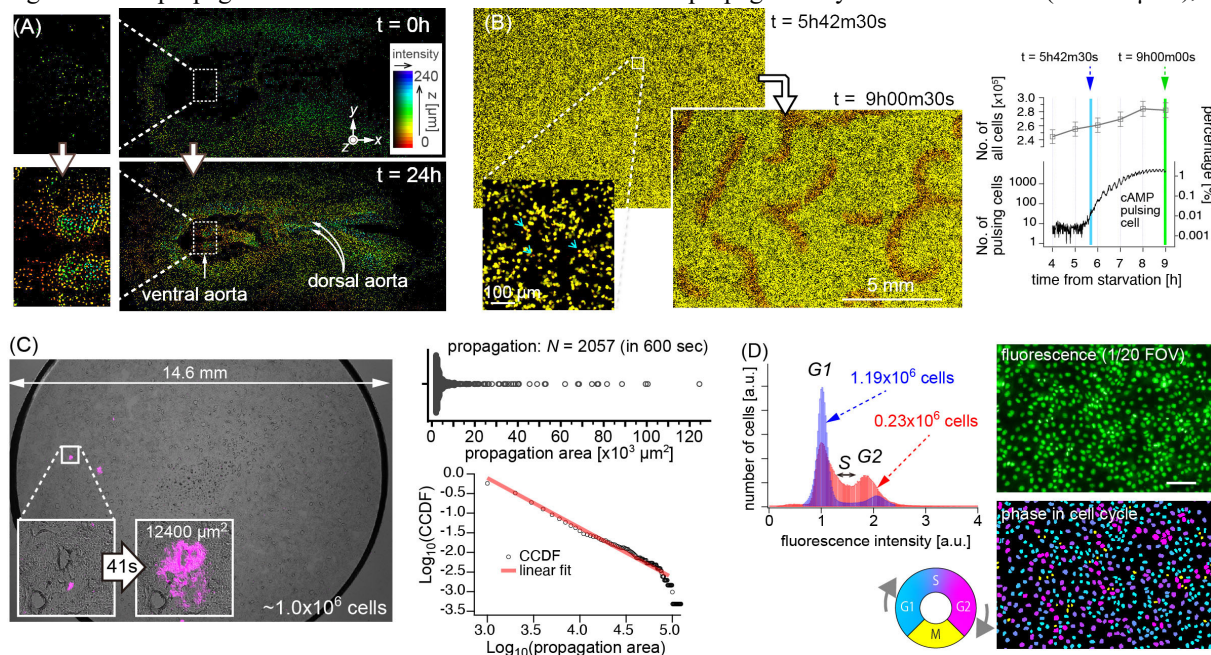
Figure 3 Applications of AMATERAS. (A) Time-lapse observation of the vascular endothelial cells in tie1:H2B-eYFP transgenic quail embryo [19]. Fluorescence images of the whole embryo and the ventral aortic region at two time points with 24 h difference are shown. Pseudo-colors in individual cell nuclei indicate their vertical positions (*z*-position) as shown in the inset (right-top). (B) Time-lapse observation of the process of nutrient-depleted *Dictyosterium discoideum* generating spiral waves of cAMP to eventually form multicellular bodies. Full FOV images of two time points, 5 h 42 m 30 s and 9 h after the nutrient removal, and a magnified image of a local region are shown. Individual particles correspond to individual cells, and cells with high cAMP concentrations are represented in red (indicated by light blue arrows). (Right-bottom) Cells with high cAMP concentrations were automatically detected by an image analysis and their transitions were plotted against time. Intracellular cAMP concentration was visualized by the fluorescent indicator protein, Flamindo2-RFP [21]. (C) Calcium ion dynamics imaging of MDCK cells. Calcium wave propagations were visualized by the calcium indicator O-GECO [23]. The calcium concentration shown in magenta is superimposed on the bright-field image. (Right-top) Stripchart of propagation area of the calcium waves. (Right-bottom) Log-log plot of the complementary cumulative distribution function (CCDF) of propagation area, fitted with a linear function. (D) (Left) Histogram of the fluorescence intensity of the nucleus in the image data of MDCK cells at two different cell densities, 1.19 x 10^6 cells/FOV (the image shown in Fig. 2(D)) and 0.23 x 10^6 cells/FOV. (Right-top) Fluorescence image of 1/20 FOV at the central region and (Right-bottom) the same image colored according to cell phase.

a very small number of propagation events have an exceptionally large propagation area (Fig. 3C, right-top). We found that it follows the power law distribution (Fig. 3C, right-bottom), which is a statistical distribution that represents self-organized critical phenomena in complex systems [24,25]. Although the detailed analysis is beyond the scope of this article, this result provides a new insight into the understanding of spontaneous calcium wave propagation. Such a result was first realized by the strength-in-number of AMATERAS in this study.

While the above examples introduced statistics for selectively detected minority cells, AMATERAS also has great potential for analyzing the statistics for all cells, including majority cells. Figure 3D shows the results of nuclear DNA content analysis after observing 1 million cultured cells (the image data shown in Fig. 2D). The fluorescence intensity of the nuclei of individual cells was measured. The histogram of fluorescence intensity, representing DNA abundance, was found to be bimodal, indicating the distribution of phases in the cell cycle. The two peaks correspond to the *G1* and *G2* phase, respectively. A similar measurement on another sample with lower cell density showed that the phase distribution was significantly different. This difference can be explained by the fact that contact inhibition occurs in high-density cells, resulting in a lower percentage of cells transitioning from *G1* to *G2* phase. Such data are usually obtained by flow cytometry [26]. The reliability of flow cytometry is guaranteed by the large number of cells observed [27], but our method can provide similar data because the number of cells is comparable to that of flow cytometry under imaging. Moreover, information on the morphology and spatial arrangement of individual cells and their dynamics can also be obtained. If a device for selective extraction of single cells [28] or aspiration of cell contents [29] is mounted on AMATERAS, the system would function as an image sorter that can selectively isolate only cells of interest with specific characteristics.

Future Perspectives for AMATERAS

There are several perspectives for AMATERAS, both from a technological and application point of view. On the technological side, there is still much room for improvement in imaging performance (sensitivity, resolution, speed, etc.), which is the key to expanding future applications. A worthwhile development is to use this lens system for brain activity imaging by two-photon fluorescence. As mentioned in the introduction, it is difficult to achieve the full FOV of AMATERAS by single-point scanning, which is used by several mesoscopes [9–11]. However, recent innovations in optical technology, such as pulse train multiplexing technology [30] and scanless two-photon fluorescence imaging [31], keep us from losing the possibility of "two-photon AMATERAS". AMATERAS also has potential as an effective observation tool for whole-brain imaging, which has been actively developed in recent years by combination of tissue clearing and light sheet illumination techniques [18,32,33]. With its capability to encompass an entire mouse brain across-section within its centimeter-scale FOV, AMATERAS achieves comprehensive 3D brain volume mapping through depth scanning alone, eliminating the need for tiling. This method is expected to dramatically enhance the throughput of whole brain imaging. Another possible development is the incorporation of various optical and spectroscopic techniques into the AMATERAS-2 system, such as molecular vibration imaging [34], quantitative phase imaging [35], and light field imaging [36]. In addition to these optical developments, AMATERAS can also be combined with single-cell omics techniques to gain a better understanding of the molecular context of cellular states within a critical transition of multicellular systems. One potential development is the integration with spatial omics technologies [37–39], which have been attracting attention in life sciences in recent years. A possible experimental approach is to observe the dynamics by live imaging in AMATERAS and then perform spatial omics on the same sample. This would allow quantification of the spatial distribution of the cellular state and thus investigate the correlation between the cellular state and the cellular dynamics.

In terms of application, although this paper has presented several examples of applications to systems biology and developmental biology, there are many other possible directions of application. For example, diseases based on genetic mutations, such as cancer, and viral diseases are phenomena that occur extremely rarely in a cell population at the onset of the pathological state and progress beyond the self-repair functions [5,40]. A fundamental understanding of such phenomena can benefit from AMATERAS' ability to observe a large number of cells simultaneously. In addition, AMATERAS can be a very suitable observation tool for the study of artificial cell sheets in regenerative medicine, where the observation of an entire large area of the sheet with single cell resolution is desirable [41,42]. It also exhibits significant potential as a high-throughput image-based cell screening platform, uniquely suited for the comprehensive study for phenotypic responses to drugs or genetic modifications. These are just a few of the possible applications and our group has received many more research proposals. We expect that new potential applications will be discovered in the future as this technology becomes more widely known to the public.

Conclusion

This paper has reviewed the development and application of a trans scale scope AMATERAS, which is one of the key technologies for promoting Singularity Biology. The development strategy to realize imaging observation of a much larger number of cells than conventional microscopy techniques was described, and the effect of "strength in numbers" in practice was demonstrated with several examples. The development of AMATERAS was conceived driven by a clear

need in the life sciences and was finally realized through the technological development described in this paper. We started this research with a specific purpose in Singularity Biology, but over time we found various directions of application, and finally it has become a multi-purpose tool. We believe that this technology will be applied to various research fields in the future and will become one of the standard tools in the life sciences.

Conflict of Interest

T.I and T.N have patent applications related to AMATERAS. The authors declare no additional conflict of interests.

Author Contributions

TI wrote the manuscript. TI, TK, and TN reviewed and edited it. TI, TK prepared figures. TK, YS, YF prepared samples and acquired data. YS, YF, YO and KH provided comments to improve the manuscript.

Data Availability

The evidence data generated and/or analyzed during the current study are available from the corresponding author on reasonable request.

Acknowledgements

References

[1] Sun, Y. C., Sun, X. F., Dyce, P. W., Shen, W., Chen, H. The role of germ cell loss during primordial follicle assembly: A review of current advances. Int. J. Biol. Sci. 13, 449–457 (2017). https://doi.org/10.7150/ijbs.18836

[2] Sasai, Y. Cytosystems dynamics in self-organization of tissue architecture. Nature 493, 318–326 (2013). https://doi.org/10.1038/nature11859

[3] Wenzel, M., Hamm, J. P., Peterka, D. S., Yuste, R. Acute focal seizures start as local synchronizations of neuronal ensembles. J. Neurosci. 39, 8562–8575 (2019). https://doi.org/10.1523/JNEUROSCI.3176-18.2019

[4] Kawatou, M., Masumoto, H., Fukushima, H., Morinaga, G., Sakata, R., Ashihara, T., et al. Modelling torsade de pointes arrhythmias in vitro in 3D human iPS cell-engineered heart tissue. Nat. Commun. 8, 1078 (2017). https://doi.org/10.1038/s41467-017-01125-y

[5] Nakai, K., Lin, H., Yamano, S., Tanaka, S., Kitamoto, S., Saitoh, H., et al. Wnt activation disturbs cell competition and causes diffuse invasion of transformed cells through NF-κB-MMP21 pathway. Nat. Commun. 14, 7048 (2023). https://doi.org/10.1038/s41467-023-42774-6

[6] Fujioka, Y., Nishide, S., Ose, T., Suzuki, T., Kato, I., Fukuhara, H., et al. A Sialylated voltage-dependent Ca^{2+} channel binds hemagglutinin and mediates influenza a virus entry into mammalian cells. Cell Host Microbe 23, 809–818.e5 (2018). https://doi.org/10.1016/j.chom.2018.04.015

[7] Goedert, M., Spillantini, M. G. Propagation of Tau aggregates Tim bliss. Mol. Brain 10, 18 (2017). https://doi.org/10.1186/s13041-017-0298-7

[8] McConnell, G., Trägårdh, J., Amor, R., Dempster, J., Reid, E., Amos, W. B. A novel optical microscope for imaging large embryos and tissue volumes with sub-cellular resolution throughout. eLife 5, e18659 (2016). https://doi.org/10.7554/eLife.18659

[9] Sofroniew, N. J., Flickinger, D., King, J., Svoboda, K. A large field of view two-photon mesoscope with subcellular resolution for in vivo imaging. eLife 5, e14472 (2016). https://doi.org/10.7554/eLife.14472

[10] Yu, C. H., Stirman, J. N., Yu, Y., Hira, R., Smith, S. L. Diesel2p mesoscope with dual independent scan engines for flexible capture of dynamics in distributed neural circuitry. Nat. Commun. 12, 6639 (2021). https://doi.org/10.1038/s41467-021-26736-4

[11] Ota, K., Oisi, Y., Suzuki, T., Ikeda, M., Ito, Y., Ito, T., et al. Fast, cell-resolution, contiguous-wide two-photon

imaging to reveal functional network architectures across multi-modal cortical areas. Neuron 109, 1810–1824.e9 (2021). https://doi.org/10.1016/j.neuron.2021.03.032

[12] Fan, J., Suo, J., Wu, J., Xie, H., Shen, Y., Chen, F., et al. Video-rate imaging of biological dynamics at centimetre scale and micrometre resolution. Nat. Photonics 13, 809–816 (2019). https://doi.org/10.1038/s41566-019-0474-7

[13] https://www.thorlabs.com/newgrouppage9.cfm?objectgroup_id=10646

[14] Ichimura, T., Kakizuka, T., Horikawa, K., Seiriki, K., Kasai, A., Hashimoto, H., et al. Exploring rare cellular activity in more than one million cells by a transscale scope. Sci. Rep. 11, 16539 (2021). https://doi.org/10.1038/s41598-021-95930-7

[15] Ichimura, T., Kakizuka, T., Sato, Y., Itano, K., Seiriki, K., Hashimoto, H., et al. Volumetric trans-scale imaging of massive quantity of heterogeneous cell populations in centimeter-wide tissue and embryo. eLife (in press). https://doi.org/10.7554/eLife.93633

[16] Sawa, Y., Miyagawa, S. Present and future perspective of cell sheet-based myocardial regeneration therapy. Biomed Res. Int. 583912 (2013). https://doi.org/10.1155/2013/583912

[17] Priest, D. G., Tanaka, N., Tanaka, Y., Taniguchi, Y. Micro-patterned agarose gel devices for single-cell high-throughput microscopy of E. Coli cells. Sci. Rep. 7, 17750 (2017). https://doi.org/10.1038/s41598-017-17544-2

[18] Susaki, E. A., Tainaka, K., Perrin, D., Kishino, F., Tawara, T., Watanabe, T. M., et al. Whole-brain imaging with single-cell resolution using chemical cocktails and computational analysis. Cell 157, 726–739 (2014). https://doi.org/10.1016/j.cell.2014.03.042

[19] Sato, Y., Poynter, G., Huss, D., Filla, M. B., Czirok, A., Rongish, B. J., et al. Dynamic analysis of vascular morphogenesis using transgenic quail embryos. PLoS One 5, e12674 (2010). https://doi.org/10.1371/journal.pone.0012674

[20] Kakizuka, T., Hara, Y., Ohta, Y., Mukai, A., Ichiraku, A., Arai, Y., et al. Cellular logics bringing the symmetry breaking in spiral nucleation revealed by trans-scale imaging. bioRxiv (2020). https://doi.org/10.1101/2020.06.29.176891

[21] Odaka, H., Arai, S., Inoue, T., Kitaguchi, T. Genetically-encoded yellow fluorescent cAMP indicator with an expanded dynamic range for dual-color imaging. PLoS One 9, e100252 (2014). https://doi.org/10.1371/journal.pone.0100252

[22] Udagawa, T., Hanaoka, K., Kawamura, M., Hosoya, T. Characteristics of spontaneous calcium oscillations in renal tubular epithelial cells. Clin. Exp. Nephrol. 16, 389–398 (2012). https://doi.org/10.1007/s10157-012-0588-4

[23] Wu, J., Liu, L., Matsuda, T., Zhao, Y., Rebane, A., Drobizhev, M., et al. Improved orange and red Ca^{2+} indicators and photophysical considerations for optogenetic applications. ACS Chem. Neurosci. 4, 963–972 (2013). https://doi.org/10.1021/cn400012b

[24] Bak, P., Tang, C., Wiesenfeld, K. Self-organized criticality. Phys. Rev. A 38, 364–374 (1988). https://doi.org/10.1103/physreva.38.364

[25] Nivala, M., Ko, C. Y., Nivala, M., Weiss, J. N., Qu, Z. Criticality in intracellular calcium signaling in cardiac myocytes. Biophys. J. 102, 2433–2442 (2012). https://doi.org/10.1016/j.bpj.2012.05.001

[26] Pozarowski, P., Darzynkiewicz, Z. Analysis of cell cycle by flow cytometry. Methods Mol. Biol. 281, 301–311 (2004). https://doi.org/10.1385/1-59259-811-0:301

[27] Nitta, N., Sugimura, T., Isozaki, A., Mikami, H., Hiraki, K., Sakuma, S., et al. Intelligent image-activated cell sorting. Cell 175, 266–276.e13 (2018). https://doi.org/10.1016/j.cell.2018.08.028

[28] Jin, J., Ogawa, T., Hojo, N., Kryukov, K., Shimizu, K., Ikawa, T., et al. Robotic data acquisition with deep learning enables cell image–based prediction of transcriptomic phenotypes. Proc. Natl. Acad. Sci. U.S.A. 120, e2210283120 (2023). https://doi.org/10.1073/pnas.2210283120

[29] Fujii, T., Matsuda, S., Tejedor, M. L., Esaki, T., Sakane, I., Mizuno, H., et al. Direct metabolomics for plant cells by live single-cell mass spectrometry. Nat. Protoc. 10, 1445–1456 (2015). https://doi.org/10.1038/nprot.2015.084

[30] Demas, J., Manley, J., Tejera, F., Barber, K., Kim, H., Traub, F. M., et al. High-speed, cortex-wide volumetric recording of neuroactivity at cellular resolution using light beads microscopy. Nat. Methods 18, 1103–1111 (2021). https://doi.org/10.1038/s41592-021-01239-8

[31] Papagiakoumou, E., Ronzitti, E., Emiliani, V. Scanless two-photon excitation with temporal focusing. Nat. Methods 17, 571–581 (2020). https://doi.org/10.1038/s41592-020-0795-y

[32] Voigt, F. F., Kirschenbaum, D., Platonova, E., Pagès, S., Campbell, R. A. A., Kastli, R., et al. The mesoSPIM initiative: Open-source light-sheet microscopes for imaging cleared tissue. Nat. Methods 16, 1105–1108 (2019). https://doi.org/10.1038/s41592-019-0554-0

[33] Otomo, K., Omura, T., Nozawa, Y., Saito, Y., Susaki, E. A. descSPIM: Affordable and easy-to-build light-sheet microscopy for tissue clearing technique users. bioRxiv (2023). https://doi.org/10.1101/2023.05.02.539136

[34] Mochizuki, K., Kumamoto, Y., Maeda, S., Tanuma, M., Kasai, A., Takemura, M., et al. High-throughput line-illumination Raman microscopy with multislit detection. Biomed. Opt. Express 14, 1015–1026 (2023).

https://doi.org/10.1364/BOE.480611

[35] Hugonnet, H., Kim, Y. W., Lee, M., Shin, S., Hruban, R. H., Hong, S.-M., et al. Multiscale label-free volumetric holographic histopathology of thick-tissue slides with subcellular resolution. bioRxiv (2021). https://doi.org/10.1117/1.ap.3.2.026004

[36] Nöbauer, T., Zhang, Y., Kim, H., Vaziri, A. Mesoscale volumetric light-field (MesoLF) imaging of neuroactivity across cortical areas at 18 Hz. Nat. Methods 20, 600–609 (2023). https://doi.org/10.1038/s41592-023-01789-z

[37] Ståhl, P. L., Salmén, F., Vickovic, S., Lundmark, A., Navarro, J. F., Magnusson, J., et al. Visualization and analysis of gene expression in tissue sections by spatial transcriptomics. Science 353, 78–82 (2016). https://doi.org/10.1126/science.aaf2403

[38] Rao, A., Barkley, D., França, G. S., Yanai, I. Exploring tissue architecture using spatial transcriptomics. Nature, 596, 211–220 (2021). https://doi.org/10.1038/s41586-021-03634-9

[39] Yao, Z., van Velthoven, C. T. J., Kunst, M., Zhang, M., McMillen, D., Lee, C., et al. A high-resolution transcriptomic and spatial atlas of cell types in the whole mouse brain. Nature 624, 317–332 (2023). https://doi.org/10.1038/s41586-023-06812-z

[40] Kataoka, K., Shiraishi, Y., Takeda, Y., Sakata, S., Matsumoto, M., Nagano, S., et al. Aberrant PD-L1 expression through 3′-UTR disruption in multiple cancers. Nature 534, 402–406 (2016). https://doi.org/10.1038/nature18294

[41] Iseoka, H., Miyagawa, S., Fukushima, S., Saito, A., Masuda, S., Yajima, S., et al. Pivotal role of non-cardiomyocytes in electromechanical and therapeutic potential of induced pluripotent stem cell-derived engineered cardiac tissue. Tissue Eng. Part A 24, 287–300 (2018). https://doi.org/10.1089/ten.TEA.2016.0535

[42] Dominguez, M. H., Krup, A. L., Muncie, J. M., Bruneau, B. G. Graded mesoderm assembly governs cell fate and morphogenesis of the early mammalian heart. Cell 186, 479–496.e23 (2023). https://doi.org/10.1016/j.cell.2023.01.001